Supplementary Information (SI) for Reaction Chemistry & Engineering.
This journal is © The Royal Society of Chemistry 2026

Supplementary Information

Promotional Effect of Rare Earth (Er, Pr, Nd, Gd and Sm) Metals on the Photocatalytic H_2O Splitting Activity of Ni-Al doped TiO_2 Catalysts for H_2 Production

Mandari Kotesh Kumar[a,b,#], Pasham Madhavi[a,#], Chatla Anjaneyulu[a] , Misook Kang[b] and Akula Venugopal[a,*]

[a] Catalysis and Fine Chemicals Division, CSIR - Indian Institute of Chemical Technology, Hyderabad-500 007, Telangana State, India. *Corresponding author E-mail address: akula.iict@csir.res.in (Akula Venugopal) Tel.: +91-40-27193165 / +91-40-27193510; Fax: +91-40-27160921.

[b] Department of Chemistry, College of Natural Sciences, Yeungnam University, 280 Daehak-Ro, Gyeongsan, Gyeongbuk, 38541, Republic of Korea.

# Equal contribution

1. Catalyst characterization

The photocatalysts were examined by using different characterization techniques. The powder X-ray diffraction patterns of the samples were recorded by Rigaku miniflex X-ray diffractometer using Ni filtered Cu K radiation (= 0.15406 nm) in the range 2 = 10–80◦ at a scan rate of 2◦min−1with a beam voltage and beam current of 30 kV and 15 mA respectively. The Brunnauer–Emmett–Teller (BET) surface areas of samples were measured by N_2 adsorption at −196◦C in an Autosorb-I (Quan tachrome) instrument. Scanning electron microscopy (SEM) with energy-dispersive X-ray spectrometry (EDS) was conducted for surface morphology, microstructural, and elemental characterizations (SEM-HITACHI S-4800). The transmission electron microscopic (TEM) images were captured by dispersing the sample in ethanol solution which was suspended on a Cu grid (400-mesh 3.5 mm diameter) using JEOL JEM 2010 electron microscope. In a typical method of H_2-TPR about 50 mg of the calcined sample loaded in a tubular sample tube. Subsequently, 10% H_2/Ar flow was continued while increasing the temperature to 800 °C at a ramp of 10 °C min^{-1}. The total amount of H2 consumption was determined. The Fourier transform infrared spectra (FT-IR) of the samples were recorded in the range 4000–400 cm^{-1}at ambient temperature using Agilent Cary 600 FT-IR spectrometer. The electron paramagnetic resonance (EPR) spectra of the samples were recorded on a JEOL/JES-FA200 EPR spectrometer at room temperature using the X-band equipment with an operating frequency of = 9.029 GHz. Raman spectra of the samples were recorded with Horiba Jobin Yvon lab ram HR spectrometer using a = 632.81 nm laser beam excitation. The diffuse reflectance (DR) UV–Vis spectra were recorded on a UV-2000, Shimadzu Spectrophotometer equipped with a diffuse reflectance attachment with an integrating sphere consisting of the $BaSO_4$ as a reference standard. At ambient temperature the spectra were recorded in the range between 185 to 800 nm with sampling interval of 0.5 nm and a slit width of 2nm and the spectra were converted to Kubelka-Munk function. X-ray photoelectron spectroscopy (XPS) was conducted using a Thermo Scientific K-Alpha spectrometer with a monochromatic Al Kα source (1486.6 eV) to examine surface composition and elemental oxidation states. PL spectra were obtained using a Spectrofluorometer (FLUORA MAX 4P) with an excitation wavelength of 330 nm, enabling the analysis of the

photoluminescent properties of the samples across the relevant emission wavelengths. Electrochemical impedance spectroscopy (EIS) was performed using an IVIUM nSTAT (Ivium Technologies, Netherlands) with a 5 mV amplitude over a frequency range of 0.01 Hz to 100 kHz. Experimental results are reported relative to the reversible hydrogen electrode (RHE).

2. Photocatalytic activity measurements

The photocatalytic H_2O splitting experiments were carried out in an air tight quartz reactor (capacity: 150 mL) using pure water and/or in aqueous methanol solution (methanol as scavenger) at ambient temperature under the natural solar irradiation (between 10 AM to 3 PM Sunny days, Hyderabad, India) and/or in the artificial solar irradiation (Solar Simulator, 1600 W m^{-2}, artificial Sun A.M1.5 Make: Science tech, Ontario, Canada). Solar simulator equipped with a UV–visible filter, with a defined cut-off wavelength of $\lambda > 420$ nm. The photocatalytic reactions were carried out at ambient temperature. During the long-term tests (10–60 h), the reaction suspension was maintained under continuous magnetic stirring, and the temperature was monitored periodically using a thermocouple. No significant temperature variation was observed throughout the experiments. In a typical experiment, required amount of powdered photocatalyst was suspended in a 50 mL of pure water and/or the 5 vol. % aqueous methanol. The reactor was charged with the pure water and/or the aqueous methanol along with catalyst and sealed with an air tight rubber septum (Aldrich) and the solution was magnetically stirred for at least 30 min to ensure the uniformity of the system. Then the reactor was purged with high purity nitrogen gas to remove the dissolved gases in the solution and the purging continued to ensure an inert atmosphere in the reactor. Prior to the photoreaction, the suspension was magnetically stirred in the dark for 30 min to establish an adsorption/desorption equilibrium condition. Subsequently the aqueous suspension contained water and/or aqueous alcohol and photocatalyst was then irradiated by artificial light and/or natural solar light under constant stirring. At regular time intervals, the hydrogen produced was collected from the sus pension and analysed immediately by a gas chromatograph (GC) with thermal conductivity detector (TCD) using molecular Sieve 5A packed column and N2as a carrier gas.

The recycle studies were carried out to evaluate the stability of the photocatalyst for 3 cycles. The 1st cycle of experiment was carried out for ~10 h under light irradiation. After the 1st cycle, reactor was kept in the dark over-night ensuring the reactor is air-tight at room temperature. Prior to 2nd cycle, the gaseous products present in the reactor was evacuated and then purged with nitrogen gas to ensure the absence of H_2 and O_2 gas dissolved by GC analysis and the experiment was performed for 10 h. The same procedure was repeated for the 3rd cycle of experiment.

Apparent Quantum Yield (AQY) Calculation

The apparent quantum yield is calculated using:

$$AQY(\%) = 2\times N_{H2}/N_{photons} \times 100$$

where:

N_{H2} = number of H_2 molecules evolved

$N_{photons}$ = number of incident photons

3. Figures:

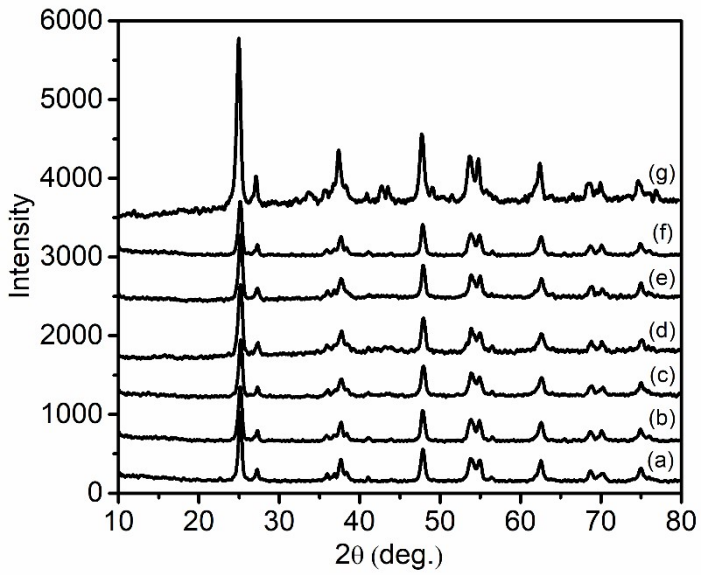

Figure S1: XRD patterns of (a) $NiAl/TiO_2$, (b) $NiErAl/TiO_2$, (c) $NiPrAl/TiO_2$, (d) $NiNdAl/TiO_2$, (e) $NiSmAl/TiO_2$, (f) $NiGdAl/TiO_2$ and (g) $P25\text{-}TiO_2$.

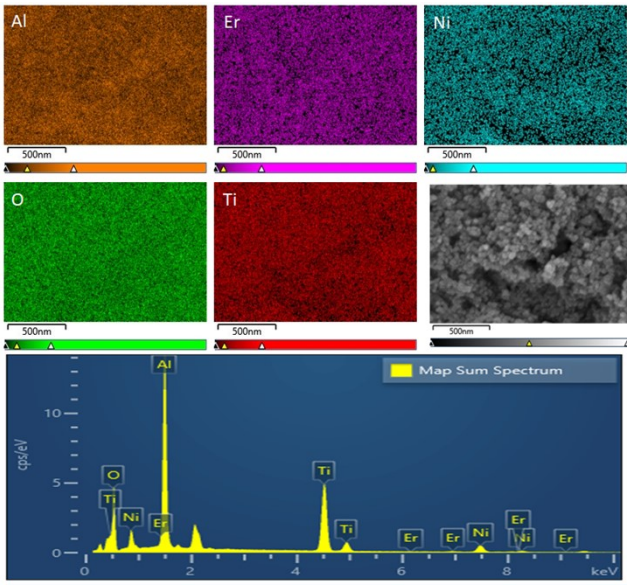

Map Sum Spectrum

Element	Signal Type	Line	Apparent Concentration	k Ratio	Wt%	Wt% Sigma	Atomic %	Standard Name	Factory Standard
O	EDS	K series	29.57	0.09949	43.42	0.28	64.54	SiO2	Yes
Al	EDS	K series	38.75	0.27831	22.22	0.14	19.58	Al2O3	Yes
Ti	EDS	K series	46.52	0.46517	24.36	0.16	12.09	Ti	Yes
Ni	EDS	K series	17.87	0.17872	9.00	0.17	3.64	Ni	Yes
Er	EDS	L series	1.50	0.01501	0.99	0.23	0.14	Er (v)	Yes
Total					100.00		100.00		

Figure S2: SEM-EDS elemental mapping of NiErAl/TiO_2; secondary electron image and analogous elemental mapping of the element Al, Er, Ni, O and Ti elements. EDS spectrum and right table for the atomic and weight percentage of various elements.

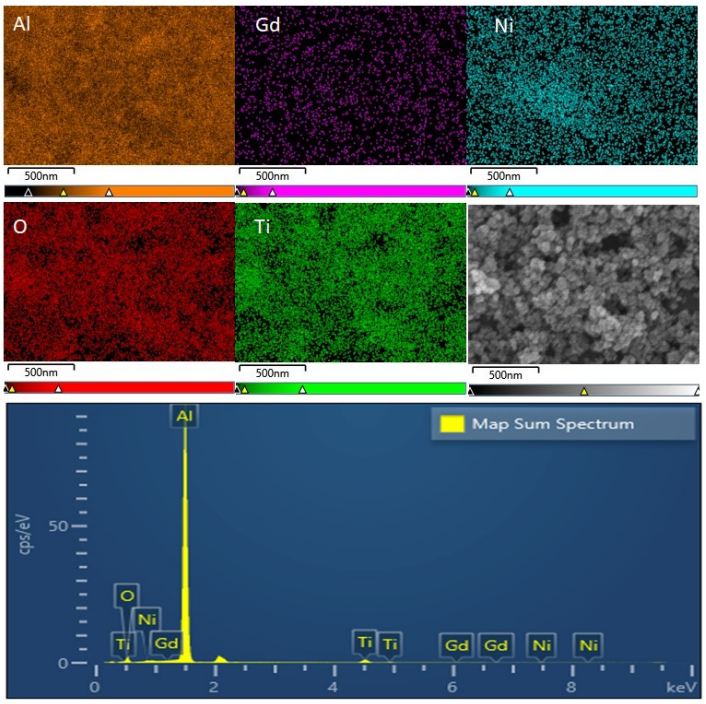

Map Sum Spectrum

Element	Signal Type	Line	Apparent Concentration	k Ratio	Wt%	Wt% Sigma	Atomic %	Standard Name	Factory Standard
O	EDS	K series	5.98	0.02013	12.78	0.19	20.27	SiO2	Yes
Al	EDS	K series	115.31	0.82818	82.03	0.23	77.15	Al2O3	Yes
Ti	EDS	K series	4.30	0.04305	4.10	0.06	2.17	Ti	Yes
Ni	EDS	K series	0.99	0.00987	0.87	0.09	0.38	Ni	Yes
Gd	EDS	L series	0.20	0.00201	0.23	0.14	0.04	Gd (v)	Yes
Total					100.00		100.00		

Figure S3: SEM-EDS elemental mapping of NiGdAl/TiO_2; secondary electron image and analogous elemental mapping of the element Al, Gd, Ni, O and Ti elements. EDS spectrum and right table for the atomic and weight percentage of various elements.

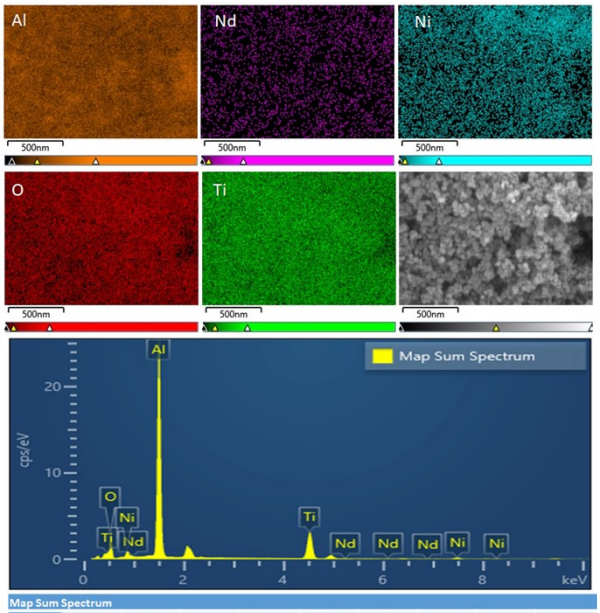

Map Sum Spectrum

Element	Signal Type	Line	Apparent Concentration	k Ratio	Wt%	Wt% Sigma	Atomic %	Standard Name	Factory Standard
O	EDS	K series	18.97	0.06382	33.45	0.24	50.20	SiO2	Yes
Al	EDS	K series	71.69	0.51490	43.51	0.18	38.72	Al2O3	Yes
Ti	EDS	K series	29.88	0.29878	19.26	0.12	9.65	Ti	Yes
Ni	EDS	K series	5.38	0.05376	3.29	0.12	1.35	Ni	Yes
Nd	EDS	L series	0.62	0.00624	0.48	0.11	0.08	Nd (v)	Yes
Total					100.00		100.00		

Figure S4: SEM-EDS elemental mapping of NiNdAl/TiO_2; secondary electron image and analogous elemental mapping of the element Al, Gd, Ni, O and Ti elements. EDS spectrum and right table for the atomic and weight percentage of various elements.

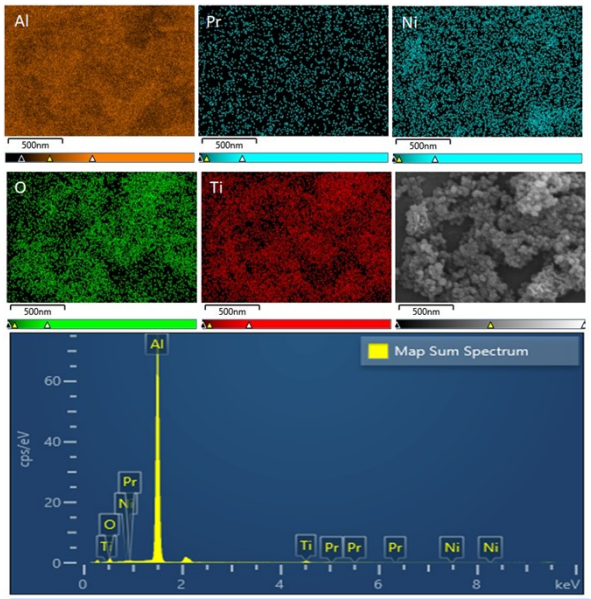

Map Sum Spectrum

Element	Signal Type	Line	Apparent Concentration	k Ratio	Wt%	Wt% Sigma	Atomic %	Standard Name	Factory Standard
O	EDS	K series	5.00	0.01684	11.22	0.20	17.81	SiO2	Yes
Al	EDS	K series	114.82	0.82471	85.68	0.24	80.61	Al2O3	Yes
Ti	EDS	K series	2.49	0.02485	2.55	0.06	1.35	Ti	Yes
Ni	EDS	K series	0.57	0.00572	0.54	0.10	0.23	Ni	Yes
Pr	EDS	L series	0.01	0.00009	0.01	0.12	0.00	Pr (v)	Yes
Total					100.00		100.00		

Figure S5: SEM-EDS elemental mapping of NiPrAl/TiO_2; secondary electron image and analogous elemental mapping of the element Al, Gd, Ni, O and Ti elements. EDS spectrum and right table for the atomic and weight percentage of various elements.

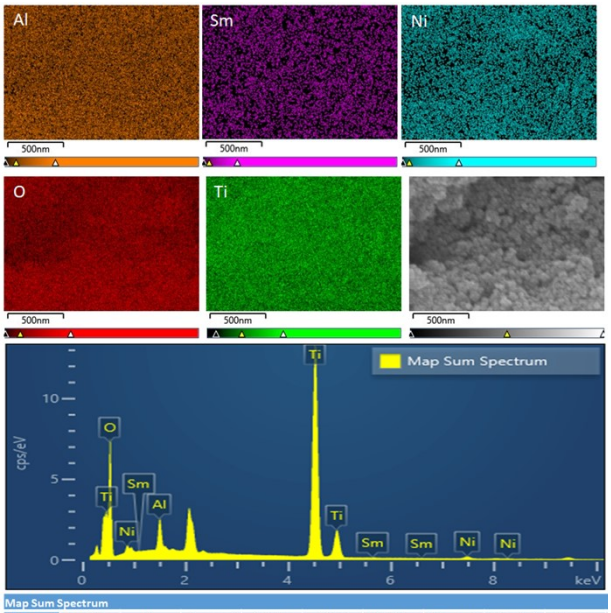

Map Sum Spectrum

Element	Signal Type	Line	Apparent Concentration	k Ratio	Wt%	Wt% Sigma	Atomic %	Standard Name	Factory Standard
O	EDS	K series	35.61	0.11982	55.47	0.18	78.41	SiO2	Yes
Al	EDS	K series	4.30	0.03086	2.04	0.03	1.71	Al2O3	Yes
Ti	EDS	K series	97.79	0.97787	40.87	0.16	19.30	Ti	Yes
Ni	EDS	K series	3.55	0.03548	1.46	0.07	0.56	Ni	Yes
Sm	EDS	L series	0.30	0.00302	0.16	0.08	0.02	Sm (v)	Yes
Total					100.00		100.00		

Figure S6: SEM-EDS elemental mapping of NiSmAl/TiO_2; secondary electron image and analogous elemental mapping of the element Al, Gd, Ni, O and Ti elements. EDS spectrum and right table for the atomic and weight percentage of various elements.

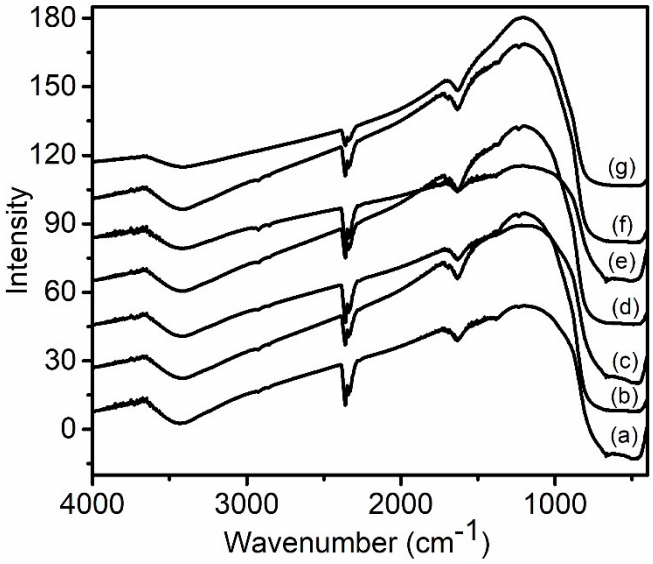

Figure S7: FT-IR spectra of (a) P25-TiO_2, (b) NiAl/TiO_2, (c) NiErAl/TiO_2, (d) NiPrAl/TiO_2, (e) NiNdAl/TiO_2, (f) NiSmAl/TiO_2 and (g) NiGdAl/TiO_2 samples.

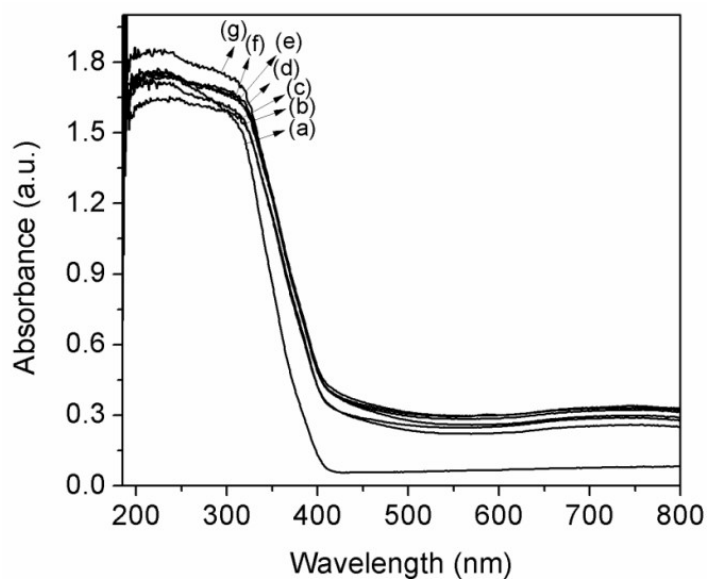

Figure S8: UV-DRS spectra of (a) P25-TiO_2, (b) NiAl/TiO_2, (c) NiErAl/TiO_2, (d) NiPrAl/TiO_2, (e) NiNdAl/TiO_2, (f) NiSmAl/TiO_2, and (g) NiGdAl/TiO_2 samples.

Table S1 Binding energy values of Rare earth doped TiO_2 samples.

Samples	O 1s	Ti $2p_{3/2}$	Ti $2p_{1/2}$	Al 2p		RE $3d_{5/2}$	RE $3d_{3/2}$
NiAl/TiO_2	529.5	458.1	463.7	68	73	-	-
NiNdAl/TiO_2	529.9	458.5	463.9	68.6	73.2	981.6	1002.3
NiPrAl/TiO_2	529.8	458.1	463.8	68.9	73.4	934.7	956.4
NiGdAl/TiO_2	529.7	458.2	463.8	67.8	73	1190.1	1216.3
NiErAl/TiO_2	529.6	458.1	463.7	67.6	72.9	169.1	178.2
NiSmAl/TiO_2	529.5	458.1	463.7	68.3	73.2	1082.1	1106.3

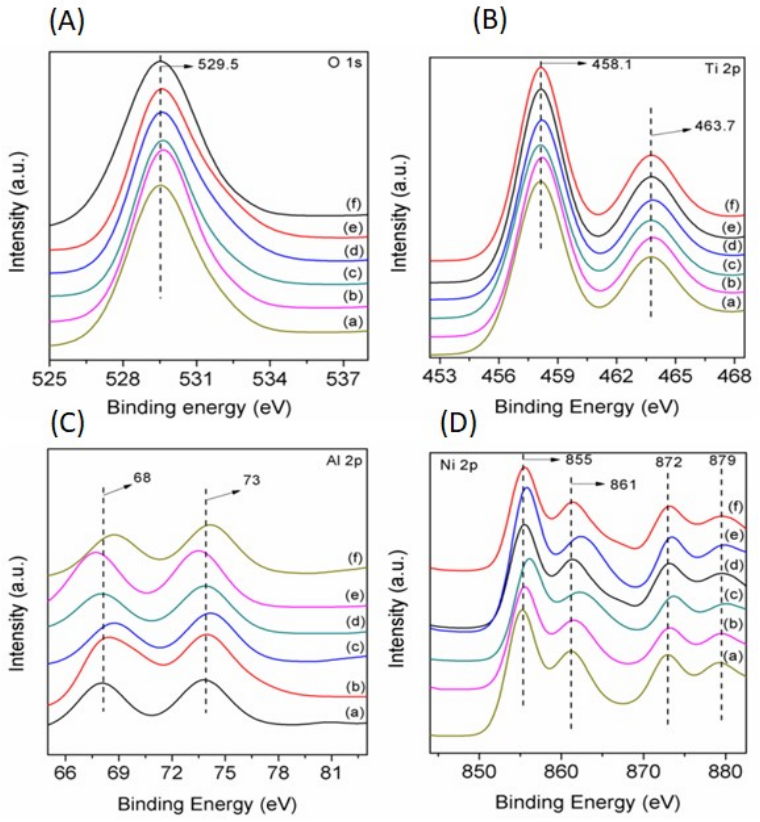
(A)
529.5
O 1s
Intensity (a.u.)
(f)
(e)
(d)
(c)
(b)
(a)
525
528
531
534
537
Binding energy (eV)
(B)
458.1
Ti 2p
463.7
Intensity (a.u.)
(f)
(e)
(d)
(c)
(b)
(a)
453
456
459
462
465
468
Binding Energy (eV)
(C)
68
73
Al 2p
Intensity (a.u.)
(f)
(e)
(d)
(c)
(b)
(a)
66
69
72
75
78
81
Binding Energy (eV)
(D)
Ni 2p
855
861
872
879
Intensity (a.u.)
(f)
(e)
(d)
(c)
(b)
(a)
850
860
870
880
Binding Energy (eV)

Figure S9 (A) O 1s, (B) Ti 2p, (C) Al 2p and (D) Ni 2p XPS patterns of (a) NiAl/TiO_2, (b) NiErAl/TiO_2, (c) NiPrAl/TiO_2, (d) NiNdAl/TiO_2, (e) NiSmAl/TiO_2 and (f) NiGdAl/TiO_2.

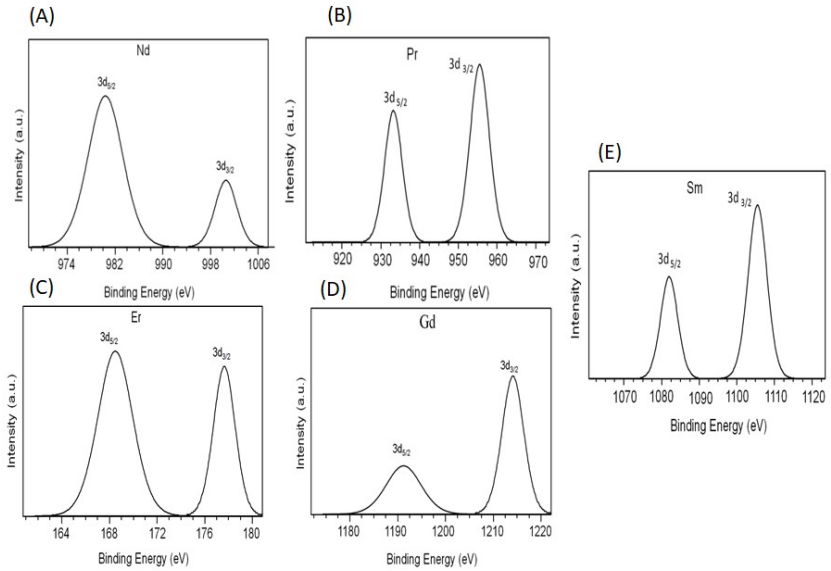

Figure S10 XPS of rare earth 3d of Nd^{3+}, Pr^{3+}, Gd^{3+}, Er^{3+} and Sm^{3+} of NiREAl/TiO_2 (RE = Er, Pr, Nd, Gd and Sm) samples.

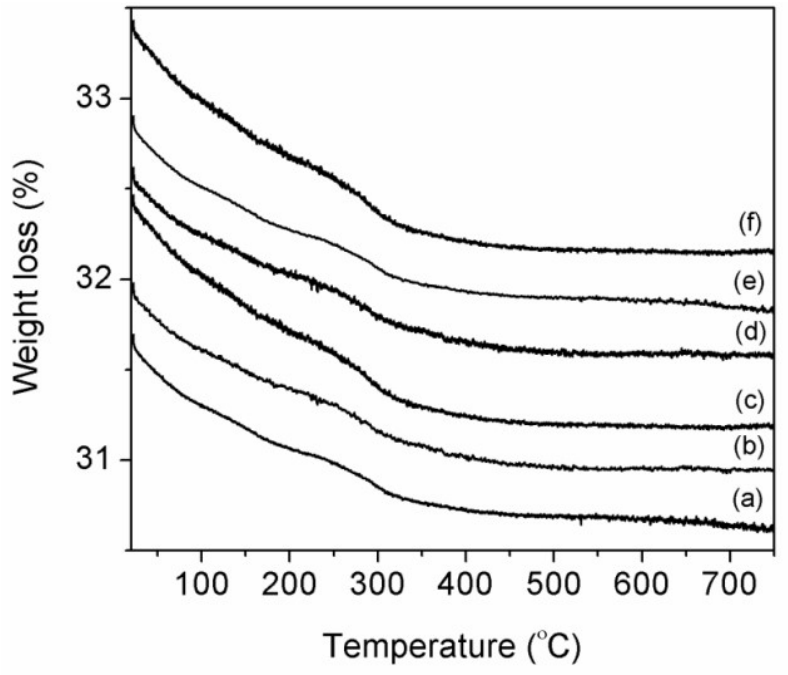

Figure S11: TGA patterns of (a) $NiAl/TiO_2$, (b) $NiErAl/TiO_2$, (c) $NiPrAl/TiO_2$, (d) $NiNdAl/TiO_2$, (e) $NiSmAl/TiO_2$ and (f) $NiGdAl/TiO_2$ samples

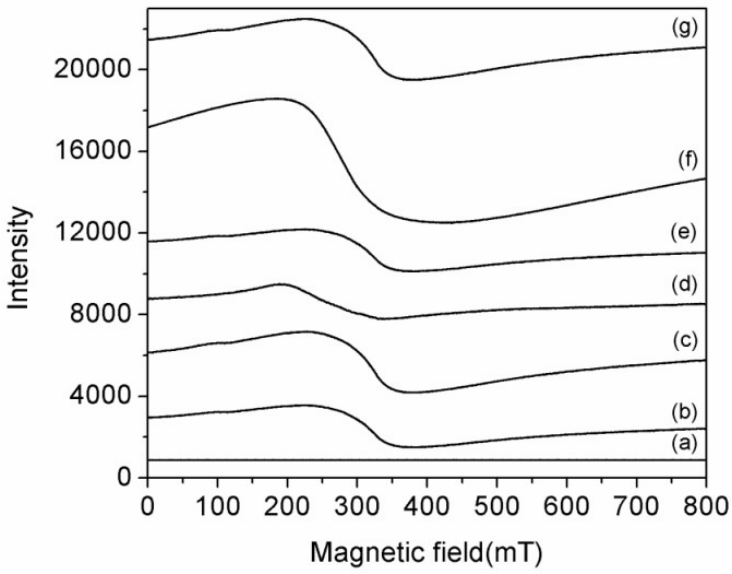

Figure S12: EPR spectra of (a) P25-TiO_2, (b) $NiAl/TiO_2$, (c) $NiErAl/TiO_2$, (d) $NiPrAl/TiO_2$, (e) $NiNdAl/TiO_2$, (f) $NiSmAl/TiO_2$ and (g) $NiGdAl/TiO_2$ samples.

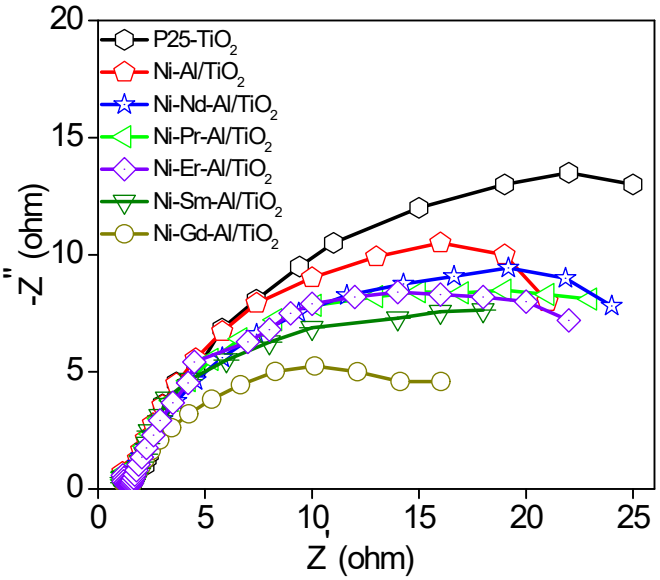

Figure S13: EIS spectra of the samples.

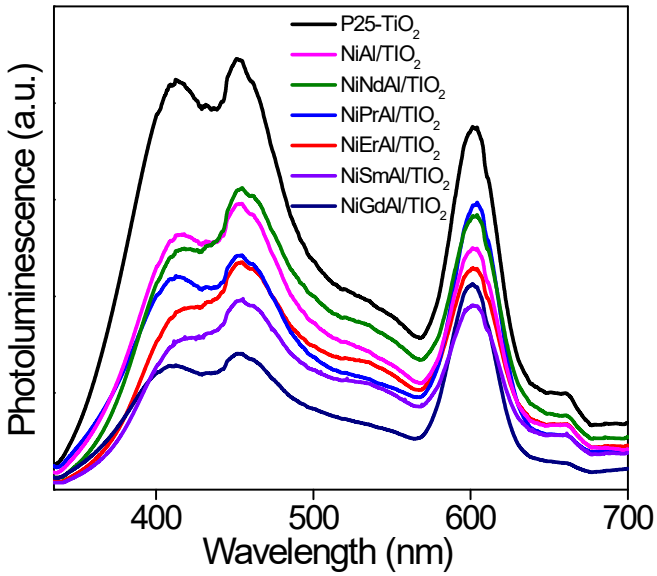

Figure S14: Photoluminescence spectra of the samples.

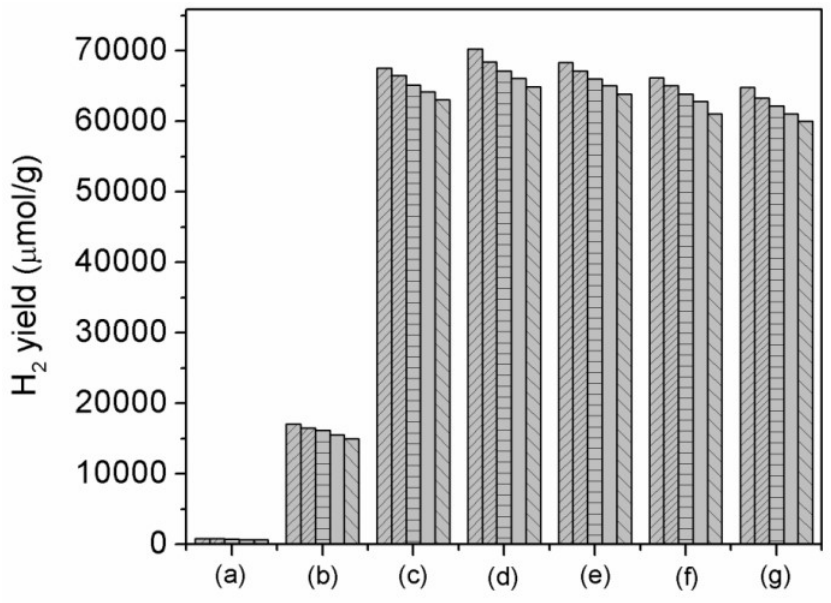

Figure S15: Recyclability tests over (a) P25-TiO_2, (b) NiAl/TiO_2 (c) NiErAl/TiO_2, (d) NiGdAl/TiO_2, (e) NiSmAl/TiO_2, (f) NiPrAl/TiO_2 and (g) NiNdAl/TiO_2 using methanol:water mixtures under solar irradiation.

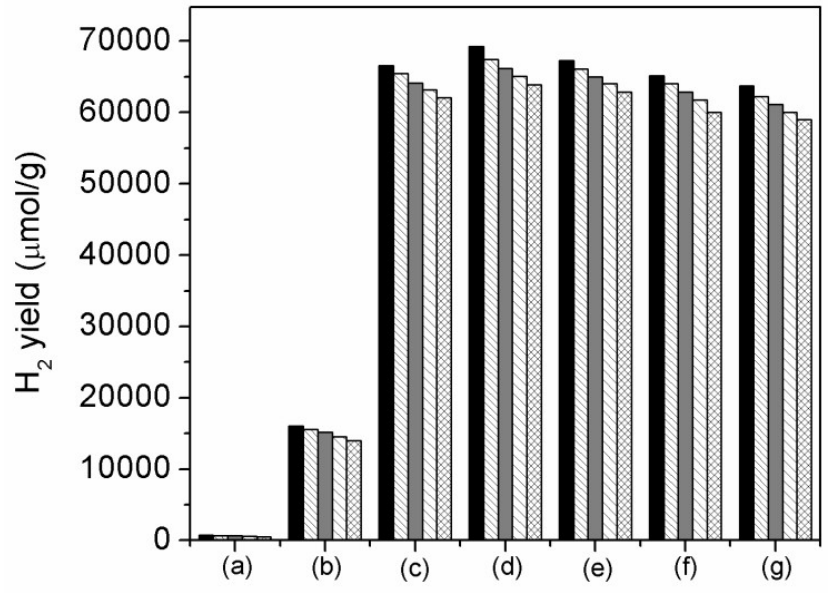

Figure S16: Recyclability tests over (a) P25-TiO_2, (b) NiAl/TiO_2 (c) NiErAl/TiO_2, (d) NiGdAl/TiO_2, (e) NiSmAl/TiO_2, (f) NiPrAl/TiO_2 and (g) NiNdAl/TiO_2 using methanol:water mixtures under artificial solar irradiation.

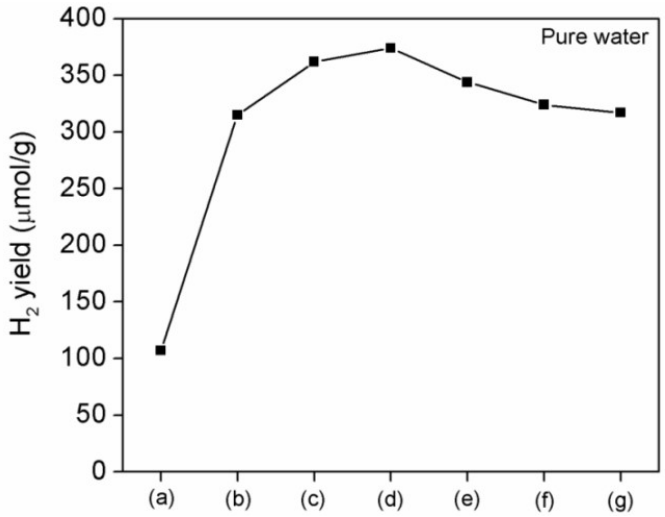

Figure S17: Photocatalytic H_2O splitting activity data over (a) P25-TiO_2, (b) NiAl/TiO_2 (c) NiErAl/TiO_2, (d) NiGdAl/TiO_2, (e) NiSmAl/TiO_2, (f) NiPrAl/TiO_2 and (g) NiNdAl/TiO_2 using tap water under natural solar irradiation.

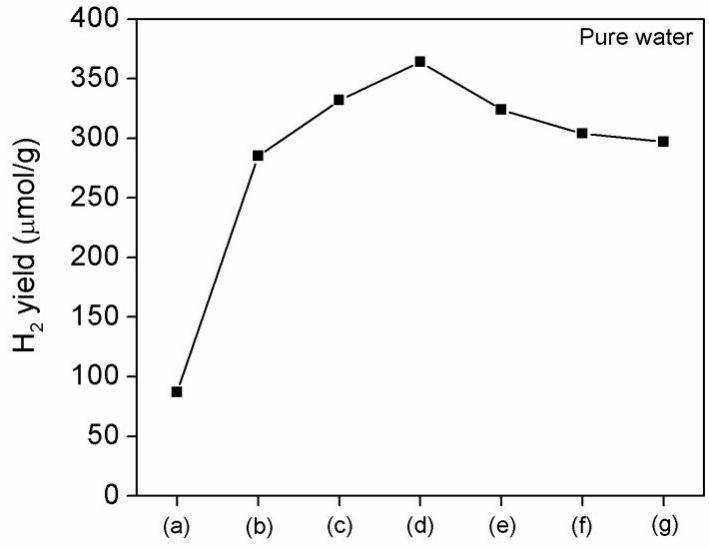

Figure S18: Photocatalytic H_2O splitting activities over (a) P25-TiO_2, (b) NiAl/TiO_2 (c) NiErAl/TiO_2, (d) NiGdAl/TiO_2, (e) NiSmAl/TiO_2, (f) NiPrAl/TiO_2 and (g) NiNdAl/TiO_2 using tap water under artificial solar irradiation.

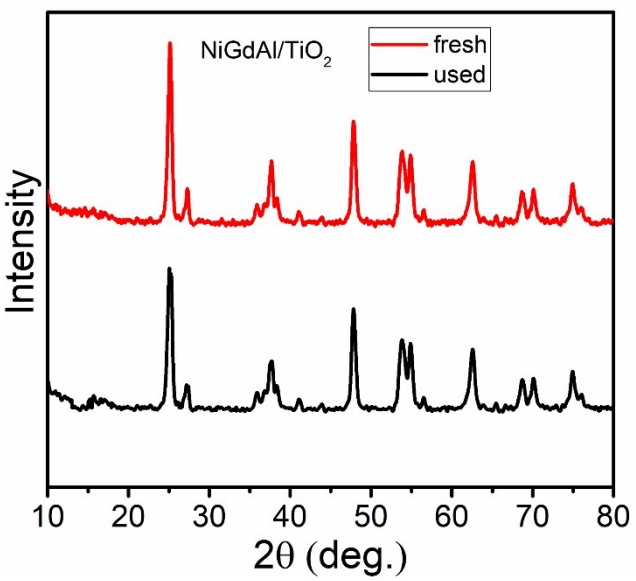

Figure S19: XRD spectra fresh and used sample of $NiGdAl/TiO_2$ after reactions under natural solar light.

Table S2: Physicochemical properties of Rare earth doped TiO_2 samples

Samples	Specific surface area (m^2/g)	Band gap (eV)	Crystallite size (nm)
P25-TiO_2	50	3.20	27.00
$NiAl/TiO_2$	112	3.12	21.5
$NiPrAl/TiO_2$	134	3.09	20.8
$NiNdAl/TiO_2$	135	3.08	20.7
$NiErAl/TiO_2$	138	3.09	20.8
$NiGdAl/TiO_2$	131	3.06	20.0
$NiSmAl/TiO_2$	140	3.07	20.6

Table S3: Comparison between H_2 evolutions of the different TiO_2 based photocatalysts

Photocatalyst	H_2 evolution (µmol g^{-1} h^{-1})	Light source	Ref.
N_2-TiO_2	103.6	Visible-Light	[1]
25 wt% $BiVO_4$/Nd-TiO_2	538.44	Visible-Light	[2]
5.0 wt% Cu0.59Ni0.41-TiO_{2-X}	389.88	Visible-Light	[3]
4 % CuSe/TiO_2	1318	Visible-Light	[4]
g-C_3N_4/TiO_2	1200	300 W Xe lamp	[5]
Cu_2Ni_1/TiO_2	285.4	Visible-Light	[6]
Pt-loaded TiO_2	105	450 W Xe lamp	[7]
SnS_2 (5 wt%) GO-RGO (0.01 wt%)	61.5	Visible light	[8]
TiO_2/CdS/TiN NRA	129.6	Visible-Light	[9]
$CuInS_2$/TiO_2/MoS_2	1034	300 W Xe lamp	[10]
Pt NCs/TiO_2	540	300 W Xe lamp	[11]
NiGdAl/TiO_2	1503.4	Visible light	This work

References

1. Z. Xu, Y. Chen, J. Zhong, J. Chen, M. Li , Q. Wang, H. Yang, Plasma surface treatment facilitated visible light-driven H_2 production over TiO_2. Surfaces and Interfaces, 36, 2023, 102626. https://doi.org/10.1016/j.surfin.2022.102626

2. J. Dai , C. Wu , J. Ma , T. Zhang , Z. Liang , J. Zhang , G. Li , K. Gong , S. H. Chang , Regulating the electronic structure to construct root-soil-like S-scheme $BiVO_4$/Nd-TiO_2 heterojunction for visible degradation and hydrogen evolution, Separation and Purification Technology, 354, 2025, 129037. https://doi.org/10.1016/j.seppur.2024.129037

3. Y. Wang , Z. Wei , Y. Wu , L. Zhang, S. Liu, K. Xu , H.H. Liu , G. Du , X. Chai , Enhanced photocatalytic H_2 evolution from glucose reforming on CuNi-decorated oxygen-vacancy-rich black TiO_2 nanosheets, Fuel, 408, 2026, 137665. https://doi.org/10.1016/j.fuel.2025.137665

4. Y. Zhu , B. Wang , J. Zhong , J. Li , X. Zheng , C. Tian , *In-situ* construction of S-scheme CuSe/TiO_2 heterojunctions with enhanced photocatalytic H_2 production

performance, Molecular Catalysis, 582, 2025, 115204. https://doi.org/10.1016/j.mcat.2025.115204

5. C. Hu, Y. K. Jhao, Y. T. Chang , L. H. Kao , K. S. Chuang , J. H. Huang , A. Wibowo , Type-II heterojunction of g-C_3N_4/TiO_2 hollow spheres for photocatalytic H_2 production and degradation of organic contaminants in water, Journal of Alloys and Compounds, 1032, 2025, 181104. https://doi.org/10.1016/j.jallcom.2025.181104

6. R. Ren , H. Yang , B. Xia , Y. Xia , J. Zhang , Q. Yi , CuNi alloy nanoparticles supported on TiO_2 nanofiber for efficient photocatalytic H_2 evolution from aqueous ammonia, Journal of Materials Science & Technology, 238, 2025, 294-302. https://doi.org/10.1016/j.jmst.2025.02.064

7. M.Umair, L. Palmisano, M. Bellardita, Comparison between the efficiency of bare and Pt-loaded TiO_2 and $ZnIn_2S_4$ for H_2 production in the presence of triethanolamine, methanol, furfuryl alcohol used as sacrificial agents, Journal of Molecular Structure, 1340, 2025, 142567. https://doi.org/10.1016/j.molstruc.2025.142567.

8. K. Perović , M. Kovačić , M. Kraljić Roković , H. Kušić , B. Genorio, U. Lavrenčić Štangar, A. L. Božić , The development of ternary-based TiO_2-SnS_2/GO-RGO composite material for photocatalytic H_2 production under Solar light irradiation, Materials Research Bulletin, 167, 2023, 112418. https://doi.org/10.1016/j.materresbull.2023.112418.

9. J. Li, L. Wang, W. Wang, X. Jia, Y. Zhang, H. Yang, Y. Li, Q. Zhou, Cooperative effects of surface plasmon resonance and type-II band alignment to significantly boost photoelectrochemical H_2 generation of TiO_2/CdS/TiN nanorod array photoanode, Applied Catalysis B: Environmental, 334, 2023, 122833. https://doi.org/10.1016/j.apcatb.2023.122833.

10. Y. J. Yuan, G. Fang, D. Chen, Y. Huang, L.X. Yang, D. P. Cao, J. Wang, Z. T. Yu, Z. G. Zou, High light harvesting efficiency $CuInS_2$ quantum dots/TiO_2/MoS_2 photocatalysts for enhanced visible light photocatalytic H2 production, Dalton Trans., 2018, 47, 5652-5659. https://doi.org/10.1039/C8DT00356D

11. Z. X. Huang, C. Ma, F. G. Zhang, Q. Cheng, Q.Y. Liu, Y. J. Yuan, X. Zhang Sub-10 nm anatase TiO_2 nanoparticles for rapid photocatalytic H_2 production from lignocellulosic biomass, J. Mater. Chem. A, 2023, 11, 7488-7497. https://doi.org/10.1039/D3TA00553D